Thermodynamic and kinetic study of synthesised graphene oxide-CuO nanocomposites: A way forward to fuel additive and photocatalytic potentials

Saba Sehar[1], Farooq Sher[2,*], Shengfu Zhang[3,4], Ushna Khalid[1], Jasmina Sulejmanović[5], Eder C. Lima[6]

[1]*Department of Chemistry, University of Agriculture, Faisalabad 38000, Pakistan*
[2] *School of Mechanical, Aerospace and Automotive Engineering, Faculty of Engineering, Environment and Computing, Coventry University, Coventry CV1 5FB, UK*
[3]*College of Materials Science and Engineering, Chongqing University, Chongqing 400044, PR China*
[4]*Chongqing Key Laboratory of Vanadium-Titanium Metallurgy and Advanced Materials, Chongqing University, Chongqing 400044, PR China*
[5]*Department of Chemistry, Faculty of Science, University of Sarajevo, 71000 Sarajevo, Bosnia and Herzegovina*
[6]*Institute of Chemistry, Federal University of Rio Grande do Sul (UFRGS), Av. Bento Goncalves 9500, P.O. Box 15003, ZIP 91501-970, Porto Alegre, RS, Brazil*

[*] Corresponding author:
E-mail address: Farooq.Sher@coventry.ac.uk (F.Sher); Tel.: +44 (0) 24 7765 7754

Abstract

Rectangular shaped GO-CuO nanocomposites have gained special attention because of spectacular applications in wastewater treatment. However, due to lack of research, the fuel additive properties of GO-CuO are still unreported. A proper synthesis and characterisation methods are necessary to investigate the fuel additive properties of GO-CuO. The present research demonstrates the synthesis of graphene oxide (GO) sheets via a modified Hummers' method. Further, GO-CuO nanohybrid was prepared by fast, cost-effective, and easy to handle solvothermal approach. The crystal data such as crystal structure, unit cell parameters, space groups, crystal system, and coordinates were explained via XRD analysis. Physical and combustion properties of fuel were analysed at different concentrations (0, 20, 40, 60 and 80 ppm) of diesel-GO-CuO blend for fuel quality parameters. The flash point and fire point of pure diesel oil were observed as 78 and 80 $^{\circ}$C which were decreased to 50 and 58 $^{\circ}$C respectively at 80 ppm concentration. With GO-CuO nanocomposites the cloud point and pour point decreases until a temperature of -8°C and -19 $^{\circ}$C respectively with a pronounced decrease in the viscosity up to 1.83 mm^2/s. Further, the photocatalytic degradation of Methylene Red (MR) dye is studied with the effect of changing H_2O_2, photocatalyst and dye concentrations with time. Remarkably, the reaction kinetics and MR degradation of about 94% with sixth time recyclability were observed. The results of this study showed improved MR degradation when using GO-CuO with H_2O_2. GO-CuO applications can be utilised to remove other dyes in future and to improve fuel quality parameters.

Keywords: Nanohybrid; Graphene oxide; Fuel additive; Photocatalysis; Crystal structure and Photocatalytic potentials.

1. Introduction

Nowadays, fuel energy is the backbone of countries progress and mainstay of the automobile industry. Recently, the issues such as; lavish fuel prices, depletion of crude oil resources, high growth rate, low engine performances and elevated threats of global warming have been raised throughout the world. These alarming circumstances necessitated focused research on fuel quality, efficiency, and consumption improvements. The physicochemical properties of fuel largely impact on diesel engine emissions and performance. Improved physicochemical properties of diesel may lead to lower environmental pollution by decreasing unburned fuel contents, hazardous gases and increased available energy contents from the fuel [1, 2]. In this scenario, metal and organic oxides (ZnO, SnO, CuO, MnO, GO) based nanoparticles and nanocomposites can improve physicochemical properties with the reduction in unburned hydrocarbons (UHCs) and conversion of CO into greenhouse gas (CO_2) [3].

On the other side, industrialisation produce sources of dyes contaminated water and continuously released hazardous waste, threatening environmental safety and living organisms. Due to improper handling of synthetic and organic dyes from industrial wastewater, dyes could easily be detected from watercolour [4]. About 7×10^5 tons of dyes are produced annually from industries, and 15% dyes effluents are released in an open environment. The aromatic and azo (-N=N-) structures of dyes are complicated for degradation due to their structural stability. Biodegradation, membranes mechanism, coagulation, adsorption and photocatalysis are up to date techniques used for industrial wastewater treatment of dyes (Methylene red, Brilliant green, Congo red and Methylene blue) [5, 6]. Among the available techniques, photocatalytic degradation is extensively used for dye removal due to low cost, inhibition of secondary pollutants and removal of colour with complete degradation of organic pollutants. Photocatalysis produces electron-hole pairs and initiates the photoreaction by generating OH free radicals [7, 8].

Transition metal oxides such as; TiO_2, ZnO, SnO, Fe_2O_3, Al_2O_3, Co_2O_3 and CuO are used as photocatalysts and fuel additives because of their high volume to size ratio, thermal conductivity and surface area [9-13]. However, these metal oxides suffer high bandgap, low quantum efficiency, toxicity, high electron-hole recombination, solar light inactivity and cost inefficiency [14]. Among these CuO has high solar absorption with cost efficiency, nontoxicity, photocatalytic and fuel additive properties [15, 16]. Although CuO has less photocatalytic activity irrespective of low bandgap (1.2 eV), it is due to electron-hole recombination and separation resistance after photocatalysis. This defect can be improved by combining CuO nanoparticles with materials having electron-accepting and magnetically separable properties [17-19]. It has been discovered that mixing of semi-porous zeolites, silica, alumina and carbon-containing material like co-adsorbent with a metal photocatalyst, produced improved photocatalytic hybrids. GO as an excellent material has a high oxygen and electrons availability with electron transfer ability showed improved photocatalytic and exceptional magnetically separable properties [20]. GO-CuO exhibit quantum-kinetic properties in photocatalysis due to large electronic bandgap which inhibit electron-hole recombination. Metal ions and organic compounds bind with oxygen-carrying groups attached on the GO surface via electrostatic interactions and chemical coordination [21]. On the other side oxygen-carrying, a functional group in GO increases the distance between hydrophilic carbon layers and oxidise fuels to enhance its thermal properties. Hummers' method with some modifications is extensively used to synthesise high oxygen content GO sheets [22].

Thus GO incorporated by transition metal (Co, Cu, Ni, and Fe) oxides display unique synergistic properties. Variety of methods reported for the preparation of GO-CuO nanocomposites such as noncovalent, wetness impregnation, covalent reaction, hydrothermal, chemical electrolysis, solvothermal, electrophoresis, physical mixing and electrochemical deposition. Hydrothermal and solvothermal methods attain superiority due to controlled size and shape of nanostructure [23]. A very innovative study synthesised nanostructures of GO-CuO and calculated their sensors catalytic ability for dopamine deficiency and biomedical applications to kill microbes [24]. It has been studied that G-CuO nanocomposite has 4.84 times greater photocatalytic potential for MB dye as compared to CuO [25]. It has also been studied that Cu_2O-RGO have 99% initial lithium-ion battery discharge for consecutive 25 cycles and Cu_2O behave as conversion electrode [26]. Graphene-based CuO nanocomposites are extensively used as a photocatalyst, biomedical and lithium-ion batteries applications, however, the best of our knowledge no research has been carried out yet on GO-CuO for the fuel additive applications.

In contrast to previously reported studies, the need for this research work was to produce GO-CuO nanocomposites for the diesel fuel quality enhancement and photocatalytic degradation of MR organic dye. For this purpose, synthesised GO-CuO act as a diesel oil additive. To the best of our knowledge, GO-CuO nanocomposites have never been implemented as a fuel additive and organic dye degradation process at the same time. In this study, GO sheets were prepared and anchored on the extensive surface of GO by solvothermal approach. Furthermore, its applications to enhance the fuel quality mainly focusing on important fuel parameters such as; fire point, flashpoint, cloud point, pour point, kinematic viscosity and specific gravity were studied. MR was selected as dye pollutant for evaluating the dye degradation capability of GO-CuO at optimum conditions of time, catalyst dose, H_2O_2 and dye concentration.

2. Experimental

2.1 Chemicals

Graphite powder, sulphuric acid (H_2SO_4), sodium nitrate ($NaNO_3$) and potassium permanganate ($KMnO_4$), copper chloride ($CuCl_2$. $2H_2O$), sodium hydroxide (NaOH), ethanol (98%), and ethylene glycol were purchased from Sigma Aldrich (USA) and used as such without further purification. De-ionised water (DI) was used in all synthesis methods.

2.2 Preparation of GO-CuO nanocomposites

GO sheets were synthesised via a modified Hummers' method [27]. First of all graphite powder (3 g) and $NaNO_3$ (1.5 g) were dissolved in cold conc. H_2SO_4 (180 mL) and kept in an ice bath with continuous stirring for 1 h. At this stage, fine powdered $KMnO_4$ (18 g) was added to oxidise graphite with continuously mixing at 15 °C. The brownish-green solution was then stirred without an ice bath for 2 days at 50 °C until it became thick brownish paste. After this, distilled water (100 mL) was slowly dropped into the solution. In order to prevent oxidation, 30% H_2O_2 (60 mL) and distilled water (500 mL) were added to minimise the effect of $KMnO_4$. Finally, thick brownish material was settled down and centrifuged at 3600 rpm with distilled water to maintain a pH 7 of the given residues. In the end, the precipitates were dried in an electric oven at 60 °C for 2 h to obtain fine GO sheets via a modified Hummers' method [28].

Eq. (1) illustrated the preparation of CuO nanoparticles via copper chloride ($CuCl_2$) as precursor during the co-precipitation method [29]. At the first stage, $CuCl_{2.}2H_2O$ salt (9 g) was dissolved in ethanol (10 mL) and stirred for 40 min to prepared solution A. The solution B was prepared via NaOH (5.4 g) mixing into ethanol (10 mL). Solution A and B gradually mixed and kept on stirring. Stirring turned green solution to bluish-green and finally into thick black CuO precipitates. Finally, centrifuged the mixture with distilled water to remove sodium hydroxide impurities at pH 7. Then the sample was dried at 60°C for 2 h and calcined at 500 °C for 5 h.

$$CuCl_2 + 2NaOH \rightarrow Cu(OH)_2 + 2NaCl \qquad (1)$$

Following this, GO (0.6 g) sheets dispersed in ethylene glycol (20 mL) and stirred for 45 min in a flask. A sample of CuO nanoparticles (2 g) stirred in ethylene glycol (20 mL) in another container. Both solutions were mixed and sonicated together for 45 min. After complete mixing with sonication, the material was added in Teflon lined autoclave and heated at 180 °C for 5 h by following the solvothermal reaction as shown in Eq. (2).

$$Cu(OH)_2 + GO \xrightarrow{Heat} GO - CuO + H_2O \qquad (2)$$

After a given time, the mixture was cooled in an open environment and centrifuged at 3600 rpm with ethanol washing until pH 7 was obtained. The sample was dried at 50 °C for 4 h in the oven following to calcination at 500 °C for 5 h. The schematic diagram of the synthesis process is shown in **Fig. 1** [30]. The obtained product was ready for further applications.

2.3 Characterisation

The prepared CuO and GO-CuO were analysed via XPERT-PRO diffractometer with minimum 0.001° scan step size and 2θ range of 10–80° to get XRD pattern. The amorphous samples were dispersed at the substrate and used radiations of Cu-Kα (λ=1.5417 nm) [31]. The obtained results were analysed for lattice parameter calculations with the use of MATCH 3 software. Further, VESTA was used to construct structural models of metal oxide sample. The CuO and GO-CuO having either morphology were identified at 9 kV power by the use of SEM JEOL JSM-6480A. Double beam UV visible spectrophotometer was used to measure the catalytic oxidation-reduction of MR organic dye. During the fuel additive application, APEX-JCX309 Cleveland open cup tester was used to determining the flash point and fire point values. APEX-JCX406 bomb calorimeter at GB/T213 standard was utilised to obtain the calorific value of specific concentrations such as; 0, 20, 40, 60 and 80 ppm of diesel-GO-CuO solutions. The viscosity of these solutions was measured by using ASTM D445 Ostwald viscometer [32].

2.4 Fuel additive and photocatalytic properties

The physicochemical characteristics of diesel oil were studied at laboratory scale. Characterisation of all properties was observed with the introduction of GO-CuO (0.002-0.008 mg) in 100 mL of commercial PSO diesel and prepared solutions of 20, 40, 60 and 80 ppm concentrations. Their combustion analysis was estimated by flash point, fire point and calorific values with the use of Cleveland open cup tester and Bomb calorimeter. Cleveland open cup tester has an operating temperature range as 10 to 350 °C. On the other hand, physical characteristics of these different dispersions were studied by kinematic viscosity, specific gravity, cloud point and pour point with the assistant of Ostwald viscometer, gravity meter and digital thermometer respectively [33]. The comparison between the results of different solutions for flash point, fire point, calorimetric values, cloud point, pour point, specific gravity and kinematic viscosity values are presented in **Table 1**.

The photocatalytic degradation of MR was investigated via UV-visible spectrophotometer at 200–800 nm wavelength range. The experiment was performed at constant temperature (35 °C), and at pH 8 with 1.5 M H_2O_2 added in 20 ppm dye solution in a beaker. Then 0.35 mg photocatalyst was added and kept the solution in a dark environment for 2 h to achieve the adsorption-desorption equilibrium, respectively. Later on, 3 mL of aliquot was collected step by step after a continuous interval of time and absorbance spectra were measured under a controlled environment of the spectrophotometer. The intensity of spectrophotometer was adjusted at λmax = 510 nm of MR [34]. Finally, the equilibrium adsorption capacity was calculated following the Eq. (3):

$$qe = (C_O - C_e)\,{}^{V}\!/_{W} \tag{3}$$

where C_o is initial dye concentration in ppm, Ce is equilibrium dye concentration in ppm, V is the volume of dye solution, and W is adsorbent mass in mg. Finally, the removal percentage was determined by using Eq. (4):

$$\%\,Removal = (C_O - C_e)/C_O \times 100 \tag{4}$$

The rate of dye removal was investigated with different concentration of H_2O_2 (1–3 mL), photocatalyst samples (GO, CuO and GO-CuO), specific concentrations (0.20, 0.25. 0.30 and 0.35 mg) of GO-CuO and dyes solutions (20, 30 and 40 ppm) at variable time duration from 0 to 90 min [35].

3. Results and discussion

3.1 Structural and morphological analysis

The crystal structure of GO is explained by XRD pattern and presented in **Fig. 2** (a). GO has 2θ value implies at 10.98 ° belongs to (001) plane. The XRD pattern of CuO has 2θ as 35.60, 38.90, 48.65, 61.7 and 68.16 ° corresponding to lattice planes as (002), (111), (220), (111) and (113) respectively with JCPDS number 96-901-6327 as shown in **Fig. 2** (b). The observed dimensions indicate that given CuO diffraction pattern have a monoclinic lattice structure [36]. Further, **Fig. 2** (b) illustrates the diffraction peaks of GO-CuO with 2θ values in the series of 23.20, 32.50, 35.47, 38.70 and 46.20° with corresponding crystallographic plane values of (020), (110), (002), (111) and (-112) respectively with JCPDS numbers 96-901-5925. It confirms that after solvothermal, the (001) plane of GO peak with $2\theta=10.98°$ has shifted to (020) plane in GO-CuO due to the reaction of GO with CuO metal nanoparticles. It has also been observed that GO and CuO structures have not been destroyed after their chemical combinations and agreed well with already reported planes (002) (200) and (113) for monoclinic CuO-RGO [35]. On the other hand, (110) plane have a high-intensity peak as compared to previous studies due to the use of GO without further reduction or some type of moisture contents.

There is no extra peak due to low noise ratio values. Moreover, the XRD pattern shows that the sample of nanoparticles has pure and sharp peaks, that specifies the sample is highly crystalline. Space groups, unit cell parameters, coordinates and density of CuO are explained in **Table 2**. The study of diffraction peaks illustrated that CuO has a monoclinic structure with C1 2/c1 (15) space group [37]. One Cu atom bonded with four oxygen atom in tetrahedral position and there are 22 total atoms in on unit cell as shown in **Fig. 3** (a-b) with standard atomic colours. Unit cell shows complex bonding arrangements with unique axis b in **Fig. 3** (c). One unit cell possesses six polyhedral planes, out of which four planes are shared with another unit cell as shown in **Fig. 3** (d). While **Fig. 3** (e-g) represents the orientation of (002), (111) and (220) respective plans. **Fig. 3** (h) shows all the possible lattice planes present in CuO as (111), (002), (220) and (113) successfully in one unit cell. It is observed that all the crystallographic planes pass through at least two polyhedral planes.

The morphological studies were carried out via SEM analysis of CuO and GO-CuO after calcination at 500 °C and represented in **Fig. 4** (a-d). The SEM images were collected at different magnifications such as 100, 250, 500 and 800× with viewing ranges of 50-500 µm. It has been revealed that CuO is in rectangular shaped particles having a high rate of aggregation with each other and form dispersed rectangular-shaped arrangements to lower their surface energies. The particles surfaces are rough from outside and become finer towards inwards. **Fig. 4**(e-h) illustrated highly dispersed CuO nanoparticles on the GO sheets and showed particles as sheet-like morphology. It can be identified that GO has amorphous structural morphology on which CuO nanoparticles are evenly distributed. These CuO nanoparticles are highly stacked on graphene sheets that prevent their agglomeration and stacking with each other. The observed results can also be justified well by the same trend of agglomerated nanoparticles on graphene sheets in Cu_2O/RGO [38].

3.2 Nanocomposite as a fuel additive

The flash point and fire point were determined to find out the combustion properties of diesel oil. Flash point is the lowest temperature at which a liquid starts to ignite in contact with air. While the fire point is the lowest value of temperature at which mixture a fuel starts burning [39]. Solutions of different concentrations (0, 20, 40, 60 and 80 ppm) are presented in **Fig. 5** (a) after flash point and fire point analysis. The reference solution has no concentration of GO-CuO, so displayed high-temperature values for flash and fire points. The reference values for flash and fire point were 78°C and 80°C, respectively. As the concentration of GO-CuO increased up to 40 ppm, the values of flash point decreased from 78 to 66 °C. On the other side, the decreasing trend for fire point was 80 to 69 °C at 40 ppm concentration gradient. This lowering temperature value indicates that GO-CuO is an excellent fuel catalyst and has the characteristics effect to enhance the combustion rate of diesel oil in short duration with delayed ignition.

Furthermore, GO-CuO show enhanced surface area and capability to increase the heat of evaporation of nanocomposite diesel blend. As a result, it catches combustion fire more quickly. Secondly, the high oxygen content of nanocomposite as a structural oxidiser, attribute high thermal conductivity by decreasing evaporation time and efficiently oxidises SO (sulphur oxide) and CO (carbon monoxide) into SO_2 and CO_2 during fuel combustion. In this way decreases the flash point, fire point and lower the environmental threat of pollutant gases. Zubair *et al.* [40] also studied the diesel oil for flash point and fire point with the assistance of rGO-ZrO_2 as a fuel additive. It was reported that rGO-ZrO_2 reduced the flash point and fire point values up to 52 and 60 °C. Therefore, careful handling is required even at 40 ppm concentration of the catalyst.

The present research reported the flash point and fire point at 40 ppm concentrated diesel blend of GO-CuO as 66 and 69 °C respectively. These results are better as compared to the already reported in the study of rGO-ZrO_2 [40]. **Fig. 5** (b) shows that the reference solution has attained a cloud point at -4 °C and pour point at -14 °C. The cloud point decreased rapidly for 0–80 ppm solutions up to -8°C. The pour point was also measured for declared concentration (0–80 ppm) and showed a gradual decrease from -14 to -19 °C. As the concentration of GO-CuO increases, a noticeable change occurs in values of cloud point and pour point. It decreases the intermolecular forces between the diesel molecules and as a result fuel showed restricted fluidity even at -19 °C. These observations can also be compared with decreased cloud point (2 °C) and pour point (-13 °C) values as a result of rGO-ZrO_2.

Whereas the GO-CuO nanocomposite revealed high depression in cloud point and pour point up to -8 and -19 °C respectively as compared to rGO-ZrO_2 [40]. Hence, GO-CuO may be used in cold areas to inhibit the freezing of diesel oil in automobiles. The cloudy appearance of diesel is due to wax crystals formation at low temperature that could reduce its combustion. In GO-CuO treated fuel, benzene rings show no polarity and crystallised diesel oil alkanes. Thus, increase their starting time of precipitation, modify crystal growth orientation and inhibit crystallisation. The polar CuO groups on the graphene surface restrict the wax crystals growth. Therefore, diesel fuel blended with GO-CuO easily moves through engines filter and presents excellent flowing properties.

The specific gravity of GO-CuO nanocomposite in the diesel fuel was determined at 0, 20, 40, 60 and 80 ppm concentrations. It is observed that the GO-CuO in diesel has a constant value of gravity. Different concentrations of GO-CuO were introduced in 100 mL of diesel oil. For 0 ppm solution, specific gravity was 8.27 g/cm^3 that was increased to 8.91 g/cm^3 at 40 ppm additive blend. These observations can be compared with $CaSn_3$ as a diesel additive, which reported the highest 8.55 g/cm^3 specific gravity at 40 ppm concentration [41]. These differences suggest that GO-CuO have higher gravity as compared to already reported fuel additive. When the concentration gradient increased to 80 ppm, specific gravity also increased to 9.13 g/cm^3. Sample of zero GO-CuO concentration has less specific gravity as compared to the samples of 60 and 80 ppm diesel blends as clearly seen in **Fig. 5** (c).

Kinematic viscosity is the physical resistance of a mixture to flow at a specific temperature. Different concentrations of GO-CuO analysed for diesel oil viscosity at 25 °C are illustrated in **Fig. 5** (c). Flowing resistance decreased as GO-CuO concentration increases in diesel oil. As the reference has no GO-CuO, therefore, showed much high viscosity as compared to 40 and 60 ppm GO-CuO-diesel blend. The reference solution with 0 ppm concentration of GO-CuO has 1.93 mm^2/s kinematic viscosity. However, 40 and 80 ppm diesel solutions have 1.85 and 1.83 mm^2/s values for kinematic viscosity respectively. The observed kinematic viscosity for CuO_2 (B20+100 ppm) and $CaSn_3$ as a fuel additive reported a pronounced increase as 4.71–5.69 mm^2/s and 2.68–3.30 mm^2/s respectively with catalyst concentration. The previous studies discussed this increasing trend with lubrication properties, however, GO-CuO showed alternative results with optimum volatility and burning capacities [41, 42]. As an essential need of low viscosity meets their benefits with cold conditions at 1.83 mm^2/s for 80 ppm diesel blend. It is an essential requirement of cold regions with enhanced capability of olefins to reach towards the ignition chamber for combustion. Actually, GO-CuO particles decrease the interlayer attraction between the diesel oil layers and increase the total available energy contents of fuel during combustion [32].

Furthermore, 0, 20, 40, 60 and 80 ppm doses of diesel-GO-CuO were studied to measure the calorific values with the assistance of bomb calorimeter. The GO-CuO-diesel mixture revealed an increasing trend of calorific values with GO-CuO concentration. **Fig. 5** (d) shows a continuous increase in calorimeter readings for a high concentration of nano additives in the fuel. The observed calorific values for 0 and 20 ppm solutions of GO-CuO are measured as 43542 and 45304 J/g respectively. It is due to the reason that before reaching the combustion chamber, heat contents became impoverished during the delayed ignition. After reaching to ignition stage, oxygenated GO-CuO enhances the heat contents with a rapid rate of burning and high calorific values were observed. Kalaimurugan *et al.* [42] studied the Neochloris oleoabundans methyl ester (B20) blend with diesel for calorific values at different concentrated solutions (25, 50, 75 and 100 ppm) of copper oxide. It is reported that B20 + 100 ppm blend showed 45,519 J/g calorific measurements, whereas the synthesised GO-CuO increases the calorific value up to 45,634 J/g at 80 ppm catalyst concentration even without B20.

3.3 Photocatalytic application of GO-CuO

3.3.1 Photodegradation of MR

Methylene Red dye (MR) is a member of azobenzene dyes and realistically degrades at ordinary sunlight conditions. MR has absorption maxima at λmax = 510 nm studied via photocatalytic absorptions through UV-visible spectroscopic analysis. Degradation of MR takes place due to oxidation with the photo catalytically generated free radicals [5]. The photocatalytic degradation process is carried out with the assistance of H_2O_2 catalyst and UV-visible light source. Initially, all prepared samples under photocatalytic conditions (30 mL of 20 ppm dye solution at pH 8 with GO-CuO = 0.35 mg) were studied. The absorbance of UV-visible light decreases gradually with the passage of time and the maximum absorbance peak was obtained at 510 nm as shown in **Fig. 6**.

3.3.1 Comparative photocatalysis of GO, CuO and GO-CuO

The photocatalytic degradation of MR was studied for GO, CuO and GO-CuO to compare the photocatalytic behaviours. The experiment was conducted by keeping the same conditions for all the parameters (concentration, temperature and pH). The GO-CuO represents 94% MR removal efficiency as compared to GO and CuO. It is due to the extensively large surface area of GO-CuO as compared to other photocatalysts. The comparative study follows the MR degradation order as GO (78.9%)< CuO (85.5%)< GO-CuO (94%) in 90 min at pH 8, as shown in **Fig. 7**. These results have a strong comparison to the already reported studies for degradation of MR dye with the assistance of Ag@Fe, TiO_2-WO_3 and $YMnO_3/CeO_2$ composites. Ag@Fe and TiO_2-WO_3 have 88 and 91% degradation ability in 100 and 120 min respectively. The reported results showed that $YMnO_3/CeO_2$ can remove 99% MR dye, which has much-improved photocatalysis but take 240 min. As compared to these results, GO-CuO degraded about 94% MR dye in just 90 min [34, 43, 44].

3.3.2 Effect of H_2O_2 on dye removal

During photocatalysis, H_2O_2 in optimal concentration assist the degradation process as an oxidising agent. Initially, light photons generate electron-hole pair and move electrons from the valence band to conduction band of the photocatalyst. These photogenerated electrons generate superoxide free radicals (OH) when reacting with surface oxygen and H_2O_2 molecules to enhance the photodegradation. Different concentrations (1, 2 and 3 mL) of H_2O_2 were studied with 0.35 mg GO-CuO for 20 mL dye solution at pH 8 to find the effect of H_2O_2 on percentage removal of MR. **Fig. 8** illustrates plot of removal percentage versus time. It is observed that for 1 mL H_2O_2, removal percentage limited to only 40% even after 90 min. On the other hand, 3 mL H_2O_2 can remove about 94% MR at a contact time of 90 min. The removal efficiency order of H_2O_2 appeared to follow as 1 mL < 2 mL< 3 mL respectively. These are the OH radicals in H_2O_2 molecule that help in the dye degradation process and decrease the dye concentration in industrial effluent.

3.3.3 Effect of catalyst dose in photocatalysis

Photocatalyst dosage is a critical point to observe the catalyst's capability for MR removal in the current research. Increase in the concentration of photocatalyst reduces the absorption at a low level and in turn, increases the degradation. To observe the suitable concentration of photocatalyst, 0.20–0.35 mg dose of GO-CuO with 20 ppm concentration of MR along with the addition of a constant amount of H_2O_2 (3 mL) at pH 8 was analysed. Rate of degradation at 0.20 mg dose of the photocatalyst was about 54%. However, the maximum catalytic amount (0.35 mg) exhibited a high removal efficiency of 94% with a contact time of 90 min, as shown in **Fig. 9**. It is due to the fact, a greater surface area of GO-CuO accommodates a large number of MR molecules. Further increase in photocatalyst concentration shows no pronounced increase in the degradation rate due to three main reasons; (1) combination of adsorbent particles with dye molecules, (2) saturation of active sites and (3) agglomeration of photocatalyst particles. However, it increases the absorption length of the paths diffusion. The already reported results for the degradation of MR dye via Ag@Fe composite showed 93% degradation for 56 mg/L concentration of catalyst [34]. While GO-CuO with 0.35 mg concentration has 94% capability of MR dye removal.

3.3.4 Effect of dye initial concentration

Fig.10 explains the effect of MR aqueous solutions of different concentration (20, 30 and 40 ppm) over GO-CuO under visible light at same conditions (0.35 mg photocatalyst, 3 mL H_2O_2 at pH 8). For the MR, at 20 ppm initial dye concentration, degradation capacity of GO-CuO photocatalyst was determined as 94% with a contact time of 90 min. On the other side, as dye concentration was increased up to 40 ppm, the removal capacity became limited to 50%. The removal percentage follows decreasing order for dyes solutions as 20 ppm > 30 ppm > 40 ppm at same irradiated time. In some cases, the effect of increasing concentration enhanced the photocatalytic mechanisms of degradation. It is due to the availability of a large number of active sites at the start of the reaction, which decreases over time due to blockage by the dye molecules. It is observed that when dye molecules block all the active sites, the adsorption capacity remains constant and a further increase in irritating time has no pronounced effect on the degradation as reported in previous studies. The degradation of MR has also been reported with different dye concentrations (66.30–90.20 mg/L) that showed 68% degradation at 66.30 mg/L of MR dye dosage [34].

3.3.5 Adsorption kinetics models

Pseudo-first-order kinetic model described the changes that occur in dye concentration with time at equilibrium conditions. The mathematical expression for the model is given in Eq. (5) [40]:

$$\log(q_e - q_t) = \log(q_e) - \frac{k_1}{2.303}\mathrm{t} \qquad (5)$$

According to this model, q_t and q_e parameters represent the adsorption capacity in mg/g while k_1 is the pseudo-first-order rate constant in 1/L which can be determined by plotting log(q_e-q_t) against time as shown in **Fig. 11** (a). Pseudo-second order kinetic model is extensively used to study the adsorption capacity of adsorbing material. It explains the mechanism of the process as long as the nanocomposite remains in contact with the dye solution. It can be represented by Eq. (6):

$$\left(\frac{t}{q_t}\right) = \frac{1}{k_2.q_e^2} + \frac{1}{q_e}\mathrm{t} \qquad (6)$$

In pseudo-second-order differential equation, k_2 acts as the second-order rate constant in g/mg min and can be calculated by plotting t/q_t versus time scale as shown in **Fig. 11** (b) with determination coefficient (R^2) [40]. These models were applied to determine the kinetic parameters that were illustrated in **Table 3**. The pseudo-second-order kinetics parameters such as q_e, k_2 and R^2 were determined by following the kinetic Eq. (6). The intraparticle diffusion model is also studied for GO-CuO nanocomposite as represented in Eq. (7).

$$q_t = k_{id}\sqrt{t} + C \qquad (7)$$

where q_t is the sorption capacity at time t, k_{id} is the rate constant for intraparticle diffusion and C represents the boundary thickness. The relationship can be plotted between q_t and $\sqrt{t}$ that is illustrated in **Fig. 11** (c). The linear plot for pseudo-first-order represents the determination coefficient (R^2) values as 0.95, 0.47 and 0.43 for GO-CuO, GO and CuO, respectively. On the contrary, the pseudo-second-order linear equation plot for the same samples gives high R^2

values as 0.99, 0.71 and 0.98. Similarly, for the intraparticle diffusion model, these R^2 values are; 0.97, 0.95 and 0.94. As the values related to q_e calculated, q_e experimental and rate constant are also mentioned in **Table 3**. It can be determined that pseudo-first-order represents q_e calculated value (0.23 mg/g) for GO-CuO with a vast variation from the experimental value (34.98 mg/g) of q_e.

In the case of pseudo-second-order, q_e calculated (36.36 mg/g) value is comparable with q_e experimental (34.98 mg/g). These results prove that adsorption of MR on the large surface of GO-CuO does not follow the pseudo-first-order kinetic model. Further, the comparison of determination coefficient R^2 proves the validity of pseudo-second-order model as compared to pseudo-first-order. It indicates that dye removal from experimental solutions is due to physicochemical interactions between adsorbent and dye solution. As illustrated in **Fig. 11** (d), that adsorption capacities (q_e) of photocatalysts also vary from catalyst to catalyst. GO-CuO nanocomposite represents large qe and R^2 values as compared to CuO and GO photocatalysts. GO-CuO also showed equal diffusion of MR particles around itself and bulk solution phase. Therefore, GO-CuO efficiently used as photocatalyst by following the pseudo-second-order kinetic model.

In the end, to determine the recyclability of GO-CuO, the recovery of the photocatalyst was examined with the use of H_2O_2. Fig. 12 shows about 94% removal of MR molecules successfully up to the sixth run. Reusability yield decreases to 88% up to the eleventh run, indicating the reliability of GO-CuO. It has been proved that CuO nanoparticles firmly attached on the GO surface, so used up to eleven runs with 88% MR removal ability. Further reusability decreases due to washing of catalyst with each run. The results show that GO-CuO is effective photocatalyst and have reliability towards photocatalytic degradation of MR dye. Similar trends have been observed for MR degradation with TiO_2-WO_3 (sulphated TW) and $YMnO_3$/CeO_2 that showed 88 and 90% reliability up to only fifth and fourth cycle respectively as compared to GO-CuO (94% up to the sixth cycle) [43, 44].

4. Conclusions

The solvothermal method was successfully applied to synthesise GO-CuO nanocomposites, which acted as an efficient diesel additive and photocatalyst for MR removal. The structural and morphological studies remarkably confirmed high crystallinity, synthesis of rectangular-shaped binary nanocomposite and monoclinic crystal cell geometry. The XRD patterns for GO-CuO give miller indices (020) (110), (002), (111) and (-112) respectively with 2ɵ values in the series of 23.20, 32.50, 35.47, 38.70 and 46.20^o respectively. The fuel additive utilisation exhibited effective depression in flash and fire points up to 50 and 58 ^oC respectively, while in fuel viscosity up to 1.83 mm^2/s. Therefore, it increases the flowing property even at -19 ^oC and effectively delayed the wax crystal formation with crystallisation modifications. Further, the specific gravity reaches up to 9.13 g/cm^3 at 80 ppm concentration of nanocomposite in 100 mL diesel. The photocatalytic MR removal represents 94% capability of photocatalyst even at 0.35 mg concentration of GO-CuO for 90 min and successfully used up to the sixth run. It is due to a short bandgap with an extensive surface area of GO-CuO and inhibition of electron-hole recombination. GO-CuO as easy to prepare, cost-efficient and reusable photocatalyst that could be applicable at industrial scale for the photocatalysis of other industrial dyes and fuel additive applications.

Acknowledgement

The authors are grateful for the financial supports from the Foundation for Research Support of the State of Rio Grande do Sul – FAPERGS [19/2551-0001865-7] and National Council for Scientific and Technological Development – CNPq [303.622/2017-2].

References

1. Uflyand, I.E., V.A. Zhinzhilo, and V.E. Burlakova, Metal-containing nanomaterials as lubricant additives: State-of-the-art and future development. Friction, 2019. 7(2): p. 93-116.
2. Hassan, M.H.A., et al., Kinetic and thermodynamic evaluation of effective combined promoters for CO2 hydrate formation. Journal of Natural Gas Science and Engineering, 2020: p. 103313.
3. Hoseini, S., et al., Performance and emission characteristics of a CI engine using graphene oxide (GO) nano-particles additives in biodiesel-diesel blends. Renewable Energy, 2020. 145: p. 458-465.
4. Liu, Y., et al., Rapid and high-efficiency removal of methylene blue onto low-cost activated sludge: Role and significance of extracellular polymeric substances. Bioresource Technology Reports, 2019. 7: p. 100240.
5. Waghmode, T.R., et al., Sequential photocatalysis and biological treatment for the enhanced degradation of the persistent azo dye methyl red. Journal of hazardous materials, 2019. 371: p. 115-122.
6. Sher, F., et al., Implications of advanced wastewater treatment: Electrocoagulation and electroflocculation of effluent discharged from a wastewater treatment plant. Journal of Water Process Engineering, 2020. 33: p. 101101.
7. Nuengmatcha, P., et al., Enhanced photocatalytic degradation of methylene blue using Fe2O3/graphene/CuO nanocomposites under visible light. Journal of Environmental Chemical Engineering, 2019. 7(6): p. 103438.
8. Güleç, F., F. Sher, and A. Karaduman, Catalytic performance of Cu-and Zr-modified beta zeolite catalysts in the methylation of 2-methylnaphthalene. Petroleum Science, 2019. 16(1): p. 161-172.
9. Soudagar, M.E.M., et al., An investigation on the influence of aluminium oxide nano-additive and honge oil methyl ester on engine performance, combustion and emission characteristics. Renewable Energy, 2020. 146: p. 2291-2307.
10. Upadhyay, G.K., et al., Synthesis of ZnO: TiO2 nanocomposites for photocatalyst application in visible light. Vacuum, 2019. 160: p. 154-163.
11. Yang, W., et al., Graphene oxide-supported zinc cobalt oxides as effective cathode catalysts for microbial fuel cell: High catalytic activity and inhibition of biofilm formation. Nano Energy, 2019. 57: p. 811-819.
12. Magdalane, C.M., et al., Structural and morphological properties of Co3O4 nanostructures: Investigation of low temperature oxidation for photocatalytic application for waste water treatment. Surfaces and Interfaces, 2019. 17: p. 100369.
13. Akika, F., et al., Structural and optical properties of Cu-doped ZnAl2O4 and its application as photocatalyst for Cr (VI) reduction under sunlight. Surfaces and Interfaces, 2020. 18: p. 100406.
14. Fodor, S., et al., Designed and controlled synthesis of visible light active copper (I) oxide photocatalyst: From cubes towards the polyhedrons-with Cu nanoparticles. Applied Surface Science, 2019. 484: p. 175-183.
15. Hajipour, P., et al., Chemical bath synthesis of CuO-GO-Ag nanocomposites with enhanced antibacterial properties. Journal of Alloys and Compounds, 2020. 821: p. 153456.
16. Pratheepa, M.I. and M. Lawrence, Synthesis of CuO-Reduced Graphene Oxide Nanocomposite for High Performance Electrochemical Capacitors. International Journal of Research, 2018. 5(12): p. 4519-4424.

17. Sarkar, S., et al., Magnetic properties of graphite oxide and reduced graphene oxide. Physica E: Low-dimensional Systems and Nanostructures, 2014. 64: p. 78-82.
18. Choi, J., et al., Preparation and characterization of graphene oxide supported Cu, Cu2O, and CuO nanocomposites and their high photocatalytic activity for organic dye molecule. Current Applied Physics, 2017. 17(2): p. 137-145.
19. Zarren, G., B. Nisar, and F. Sher, Synthesis of anthraquinone based electroactive polymers: A critical review. Materials Today Sustainability, 2019: p. 100019.
20. Kumar, R., et al., Self-assembled nanostructures of 3D hierarchical faceted-iron oxide containing vertical carbon nanotubes on reduced graphene oxide hybrids for enhanced electromagnetic interface shielding. Composites Part B: Engineering, 2019. 168: p. 66-76.
21. Zaaba, N., et al., Synthesis of graphene oxide using modified hummers method: solvent influence. Procedia engineering, 2017. 184: p. 469-477.
22. Wang, L., et al., Designed graphene-peptide nanocomposites for biosensor applications: A review. Analytica chimica acta, 2017. 985: p. 24-40.
23. Smith, A.T., et al., Synthesis, properties, and applications of graphene oxide/reduced graphene oxide and their nanocomposites. Nano Materials Science, 2019. 1(1): p. 31-47.
24. Kumar, S.K., et al., Highly efficient multipurpose graphene oxide embedded with copper oxide nanohybrid for electrochemical sensors and biomedical applications. Journal of Science: Advanced Materials and Devices, 2017. 2(4): p. 493-500.
25. Darvishi, M., G. Mohseni-Asgerani, and J. Seyed-Yazdi, Simple microwave irradiation procedure for the synthesis of CuO/Graphene hybrid composite with significant photocatalytic enhancement. Surfaces and Interfaces, 2017. 7: p. 69-73.
26. Lu, Y., et al., One-Pot Synthesis of Cuprous Oxide-Reduced Graphene Oxide Nanocomposite as an Anode Material for Lithium Ion Battery. International Journal of Electrochem Science, 2017. 12: p. 3941-3949.
27. Ding, J., et al., Low-temperature preparation of magnetically separable Fe3O4@ CuO-RGO core-shell heterojunctions for high-performance removal of organic dye under visible light. Journal of Alloys and Compounds, 2016. 688: p. 649-656.
28. Gong, S., et al., Learning from nature: constructing high performance graphene-based nanocomposites. Materials Today, 2017. 20(4): p. 210-219.
29. Phiwdang, K., et al., Synthesis of CuO nanoparticles by precipitation method using different precursors. Energy Procedia, 2013. 34: p. 740-745.
30. Sakthivel, B. and G. Nammalvar, Selective ammonia sensor based on copper oxide/reduced graphene oxide nanocomposite. Journal of Alloys and Compounds, 2019. 788: p. 422-428.
31. Manyasree, D., K. Peddi, and R. Ravikumar, CuO nanoparticles: synthesis, characterization and their bactericidal efficacy. Int J Appl Pharmaceut, 2017. 9(6): p. 71-74.
32. Jamil, S., M.R.S.A. Janjua, and S.R. Khan, Synthesis and structural investigation of polyhedron Co3O4 nanoparticles: Catalytic application and as fuel additive. Materials Chemistry and Physics, 2018. 216: p. 82-92.
33. Jamil, S., et al., The first morphologically controlled synthesis of a nanocomposite of graphene oxide with cobalt tin oxide nanoparticles. RSC advances, 2018. 8(64): p. 36647-36661.
34. Zaheer, Z., A.-A. Aisha, and E.S. Aazam, Adsorption of methyl red on biogenic Ag@ Fe nanocomposite adsorbent: Isotherms, kinetics and mechanisms. Journal of Molecular Liquids, 2019. 283: p. 287-298.

35. Sree, G.S., et al., Enhanced UV-Visible triggered photocatalytic degradation of Brilliant green by Reduced Graphene Oxide based NiO and CuO ternary nanocomposite and their antimicrobial activity. Arabian Journal of Chemistry, 2020.
36. Rangel, W.M., R.A.A.B. Santa, and H.G. Riella, A facile method for synthesis of nanostructured copper (II) oxide by coprecipitation. Journal of Materials Research and Technology, 2019.
37. Rao, M.P., et al., Photocatalytic properties of hierarchical CuO nanosheets synthesized by a solution phase method. Journal of Environmental Sciences, 2018. 69: p. 115-124.
38. Li, B., et al., A facile one-pot synthesis of Cu2O/RGO nanocomposite for removal of organic pollutant. Journal of Physics and Chemistry of Solids, 2013. 74(4): p. 635-640.
39. Huo, X., et al., Study on Flash-Point Measurement and Reduced Prediction Model for Ternary Extraction System. Process Safety and Environmental Protection, 2020.
40. Zubair, N.F., et al., A comprehensive thermodynamic and kinetic study of synthesized rGO-ZrO2 composite as a photocatalyst and its use as fuel additive. Journal of Molecular Structure, 2019. 1198: p. 126869.
41. Khan, S.R., et al., Template free synthesis of calcium-tin (CaSn3) bimetallic micro cubes: Characterization, catalytic activity, adsorption and additive properties. Chemical Physics Letters, 2020. 739: p. 136917.
42. Kalaimurugan, K., et al., Combustion analysis of CuO2 nanoparticles addition with neochloris oleoabundans algae biodiesel on CI engine. Materials Today: Proceedings, 2020.
43. Wang, Y. and H. Tian, Study on the construction of YMnO3/CeO2 composite photocatalyst heterostructure and photocatalytic degradation of methyl red. Optik, 2020. 201: p. 163524.
44. Patil, S., et al., Sulfated TiO2/WO3 nanocomposite: An efficient photocatalyst for degradation of Congo red and methyl red dyes under visible light irradiation. Materials Chemistry and Physics, 2019. 225: p. 247-255.

List of Tables

Table 1. Effect of GO-CuO on physicochemical fuel properties.

Parameters	**Concentration of catalyst dosage**						
	0 ppm	20 ppm	40 ppm	60 ppm	80 ppm	100 ppm	**References**
Flashpoint (°C)	78	70	66	59	50	-	This work
	71	64	60	-	-	-	[40]
Fire point (°C)	80	75	69	62	58	-	This work
	74	69	54	-	-	-	[40]
Cloud point (°C)	-4	-5	-5	-6	-8	-	This work
	7	5	2	-	-	-	[40]
Pour point (°C)	-14	-15	-15	-17	-19	-	This work
	-11	-12	-13	-	-	-	[40]
Kinematic Viscosity (mm^2/s)	1.93	1.86	1.85	1.84	1.83	-	This work
	2.68	2.86	3.30	-	-	-	[41]
Specific gravity (g/cm^3)	8.27	8.75	8.91	9.12	9.13	-	This work
	8.50	8.53	8.55	-	-	-	[41]
Calorific values (J/g)	43,542	45,304	45,380	45,524	45,634	-	This work
	43,540	-	-	-	-	45,519	[42]

Table 2. Lattice parameters from XRD analysis for CuO nanoparticles.

Parameters	**Outcomes**
Formula	CuO
Space group	C1 2/c1 (15)
Cell parameters (Å)	
a (Å)	4.69
b (Å)	3.43
c (Å)	5.13
α (°)	90
β (°)	99.65
γ (°)	90
Crystal system	monoclinic
Number of atoms	22
Coordinates x, y, z for Cu atom	0.25, 0.23, 0.000
Coordinates x, y, z for O atom	-0.01, 0.42, 0.25
Volume (Å^3)	82.47
Calculated density (g/cm^3)	6.50

Table 3. Evaluation of kinetic parameters for MR adsorption on CuO, GO and GO-CuO.

Kinetic parameters	**MR dye**		
	CuO	GO	GO-CuO
Pseudo-first order			
K_1 (1/min)	0.04	0.04	0.03
q_e calculated (mg/g)	0.18	0.16	0.23
q_e experimental (mg/g)	32.14	17.08	34.98
R^2	0.43	0.47	0.95
Pseudo-second order			
K_2 (g/mg min)	0.003	0.001	0.004
q_e calculated (mg/g)	34.84	25	36.36
q_e experimental (mg/g)	32.14	17.08	34.98
R^2	0.98	0.71	0.99
Intra particle diffusion			
R^2	0.94	0.95	0.97

List of Figures

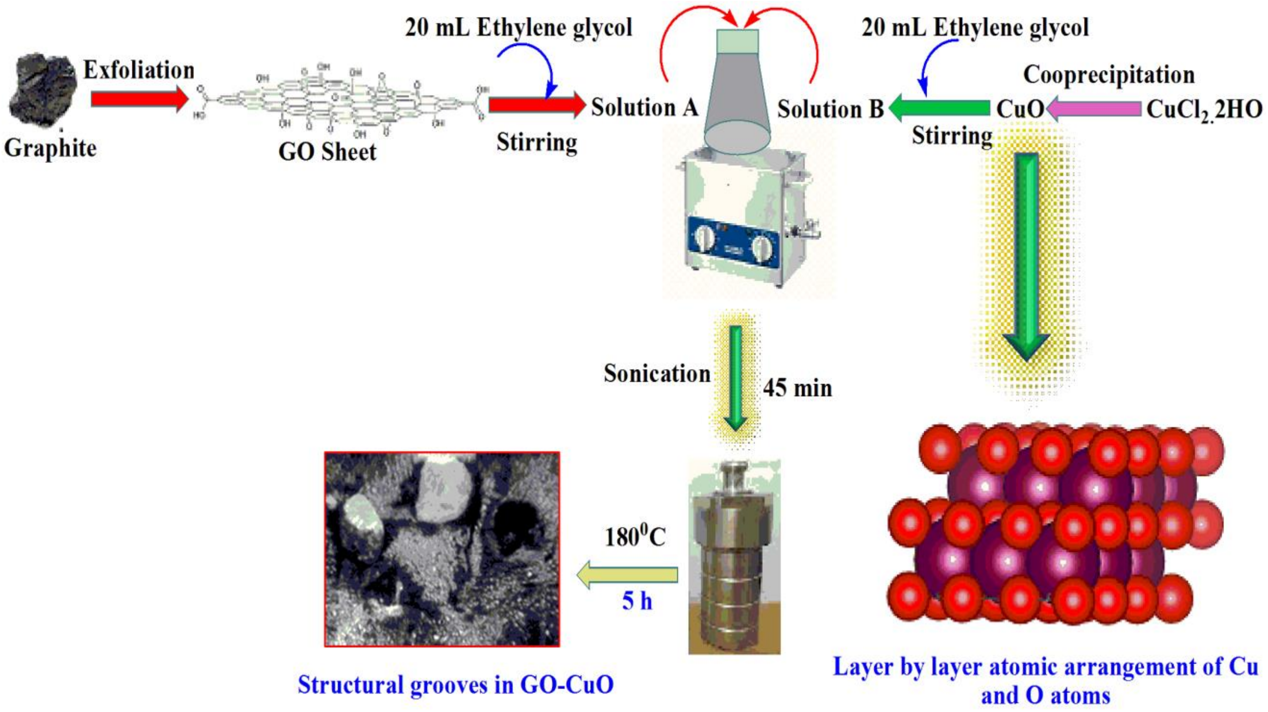

Fig. 1. Preparation scheme of GO-CuO nanocomposite.

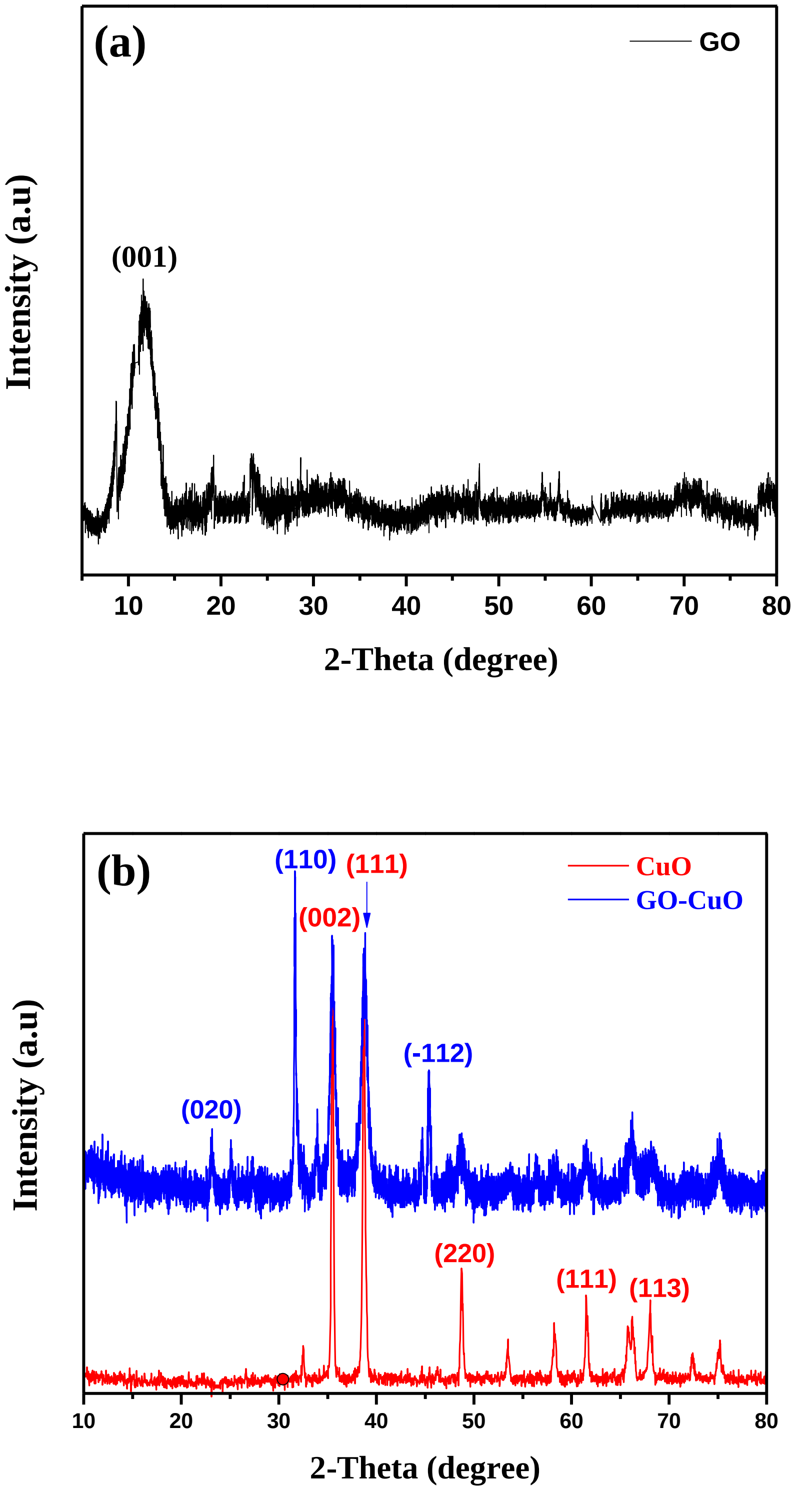

Fig. 2. X-ray diffraction patterns; (a) graphene oxide, and (b) CuO and GO-CuO.

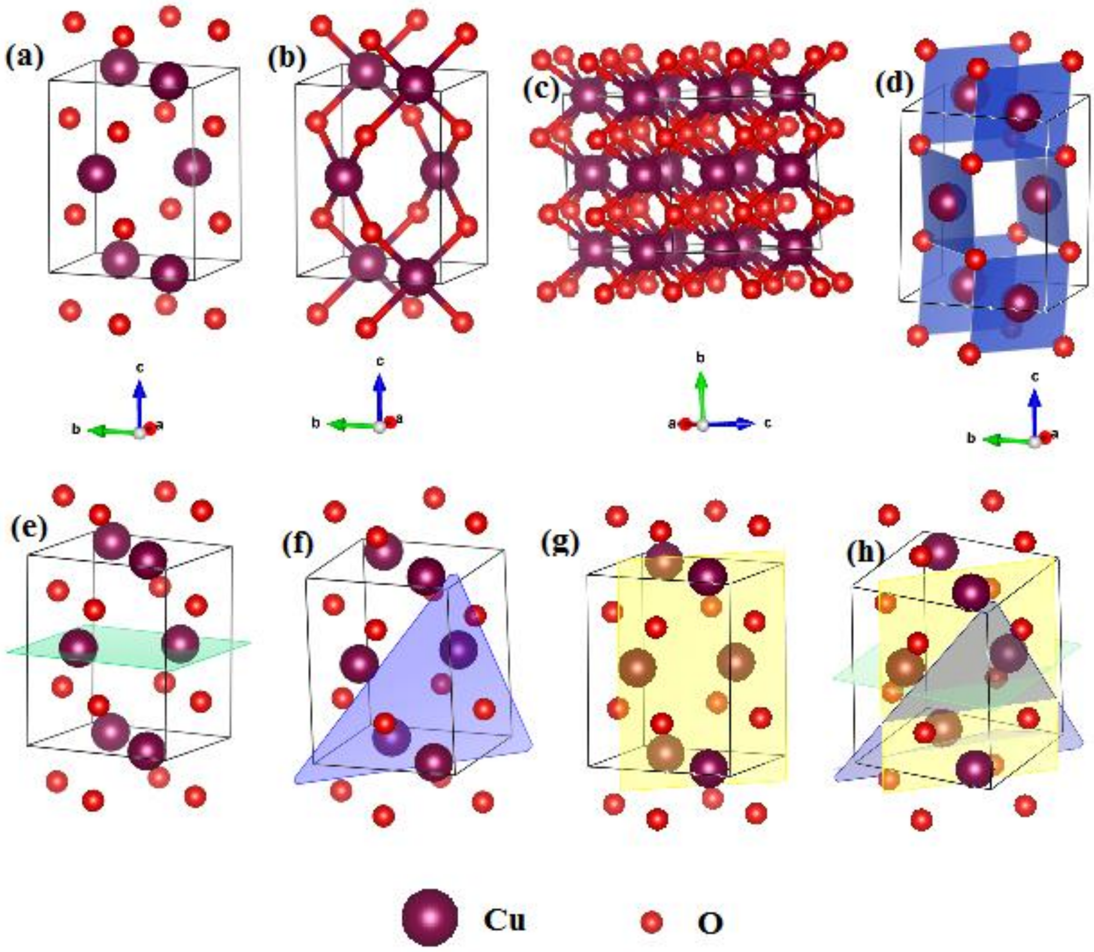

Fig. 3. Structural model of CuO; (a-b) Position of Cu and O atoms in a monoclinic unit cell, (c) atomic arrangement with unique b axis, (d) polyhedrons in unit cell, (e) unit cell representation of (002) plane with d-spacing 2.53^{o}, (f) (111) plane with d-spacing 2.32 ^{o}, (g) (220) plane with d-spacing 1.87^{o} and (h) all planes in one unit cell.

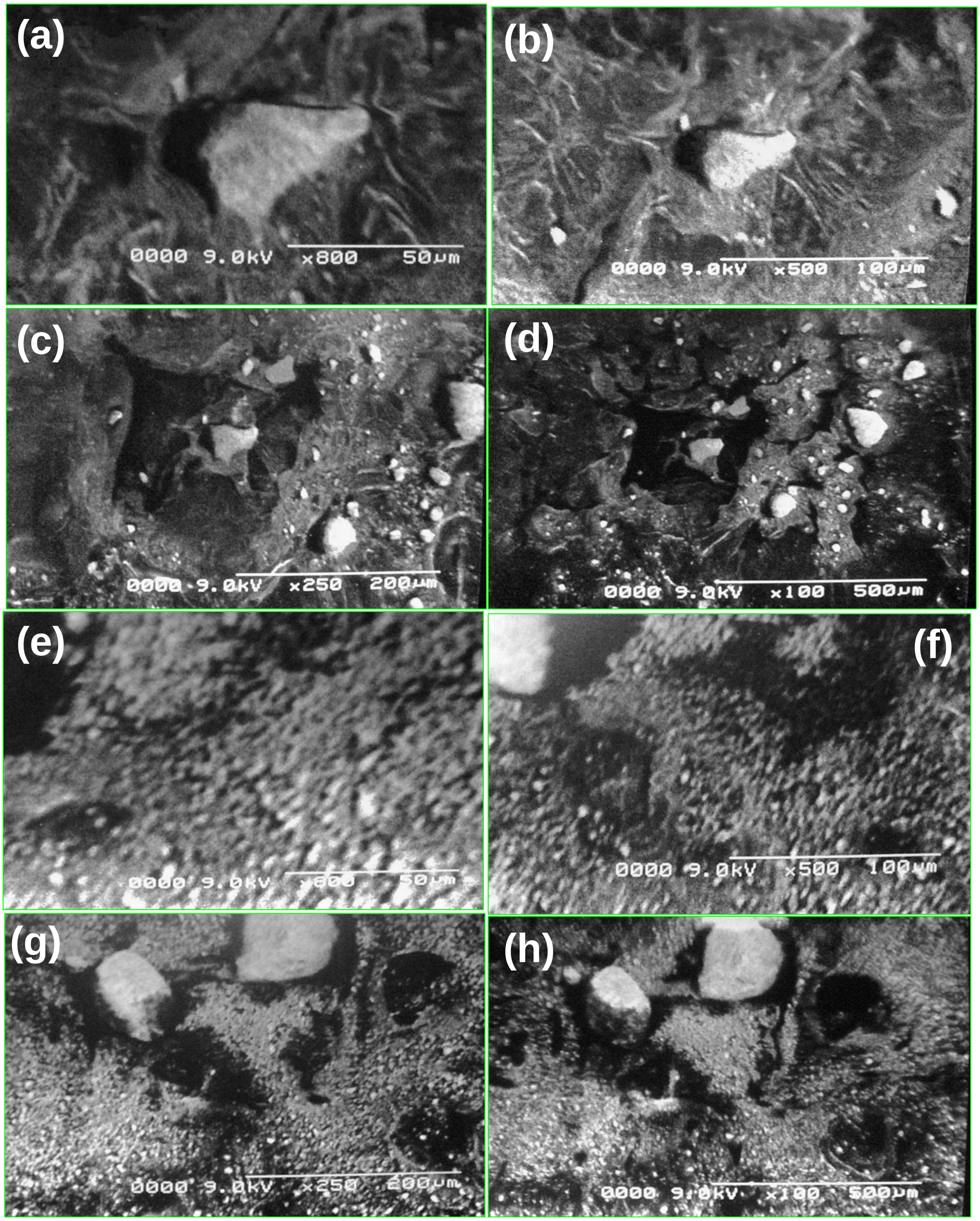

Fig. 4. SEM images of CuO nanoparticles; (a) 800× (b) 500× (c) 250× (d) 100× and GO-CuO nanocomposite at (e) 800× (f) 500× (g) 250× (g) 100×.

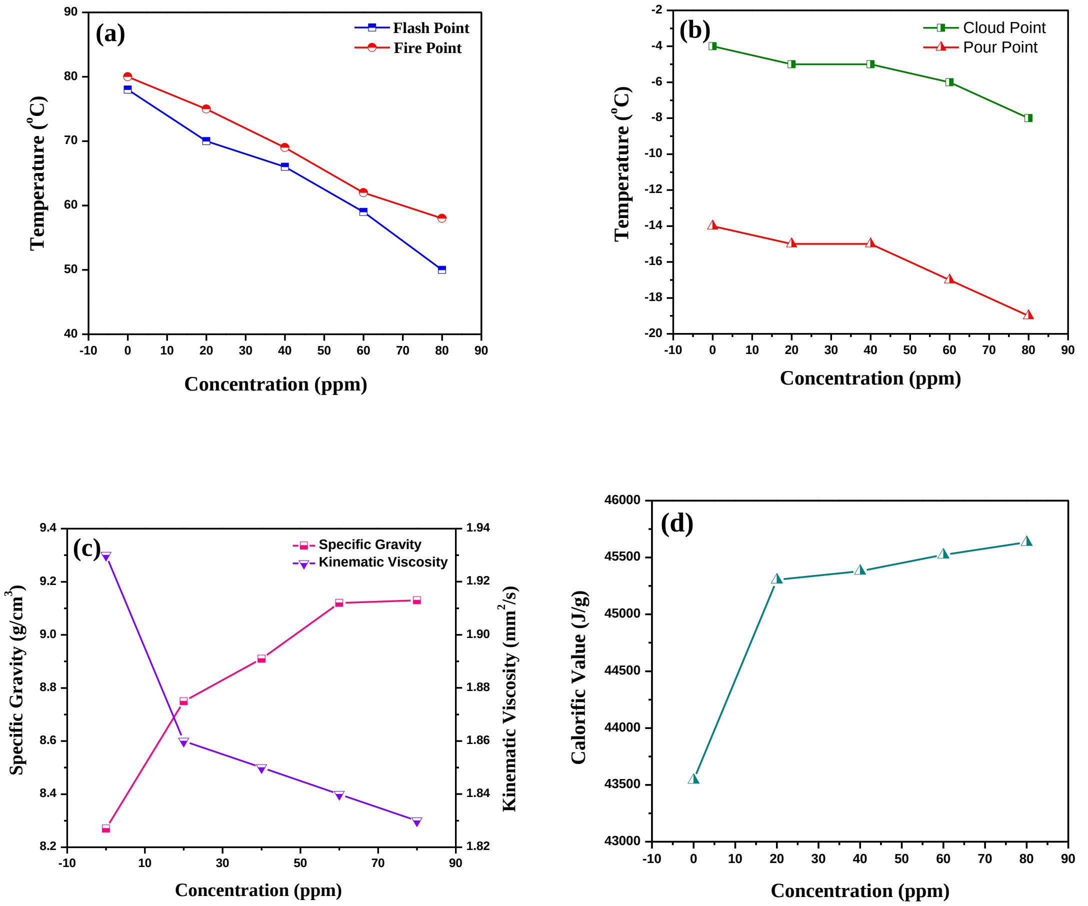

Fig. 5. Effect of GO-CuO nanocomposite for diesel oil onto; (a) flash point and fire point, (b) cloud point and pour point, (c) specific gravity and kinematic viscosity and (d) calorific value.

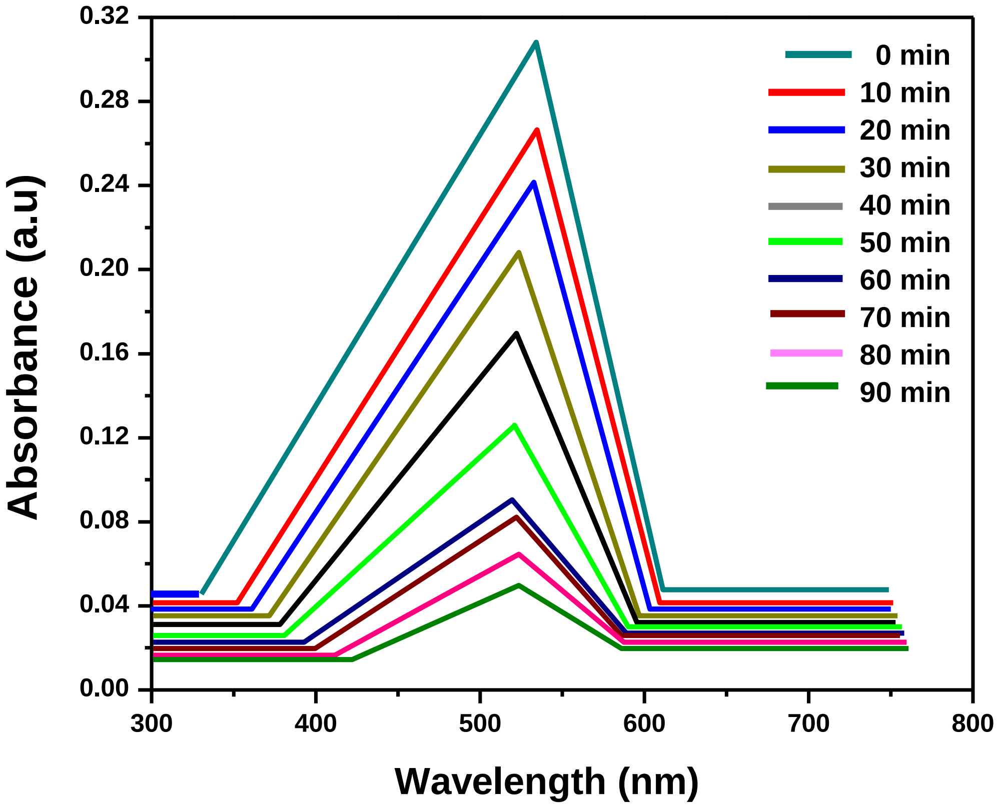

Fig. 6. Time dependent UV-visible spectra of catalytic absorbance for MR dye (conditions: [MR dye]=20 ppm, [H_2O_2]= 1.5M, [GO-CuO]=0.35 mg).

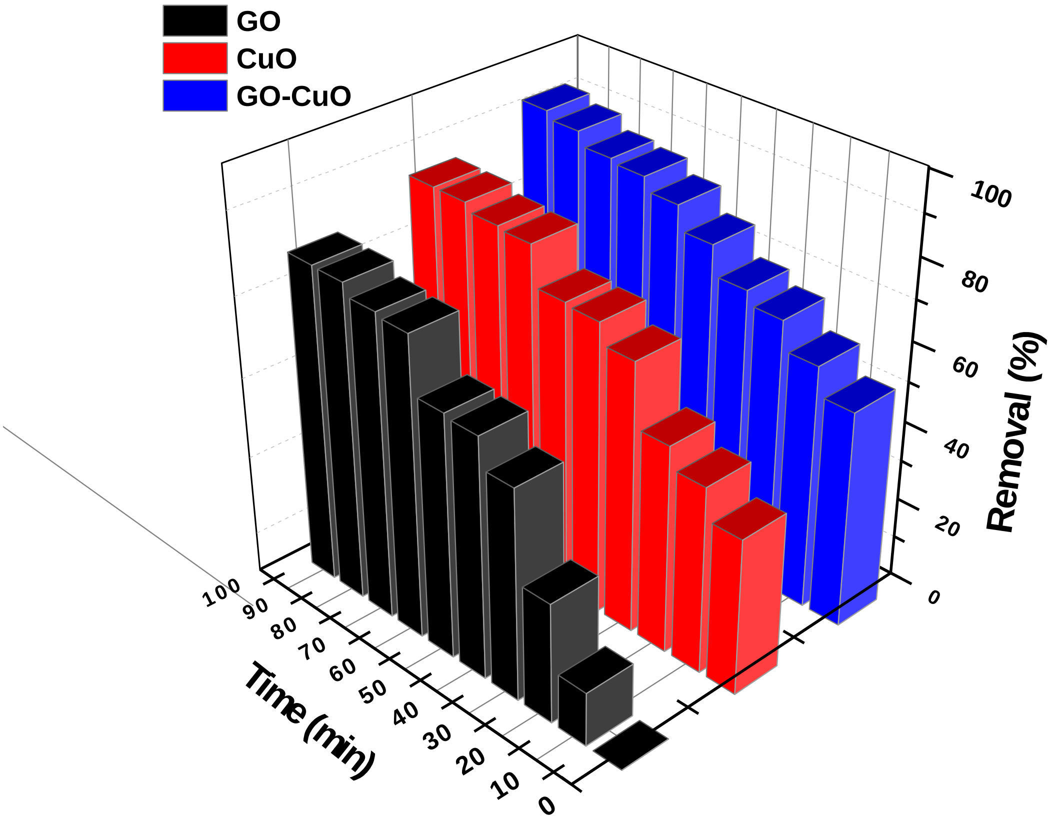

643

644 **Fig. 7.** Effect of GO, CuO and GO-CuO on the percentage removal of MR dye.

645

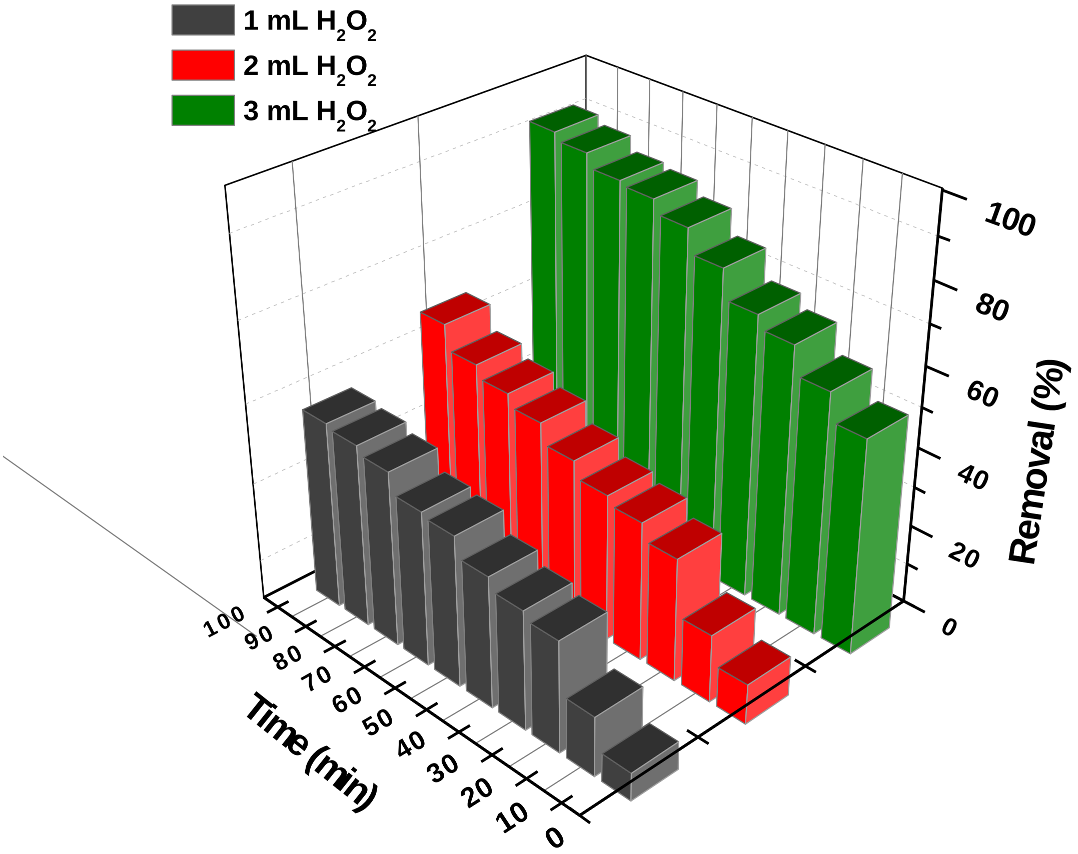

Fig. 8. Effect of H_2O_2 concentrations on the percentage removal of MR dye with GO-CuO nanocomposites.

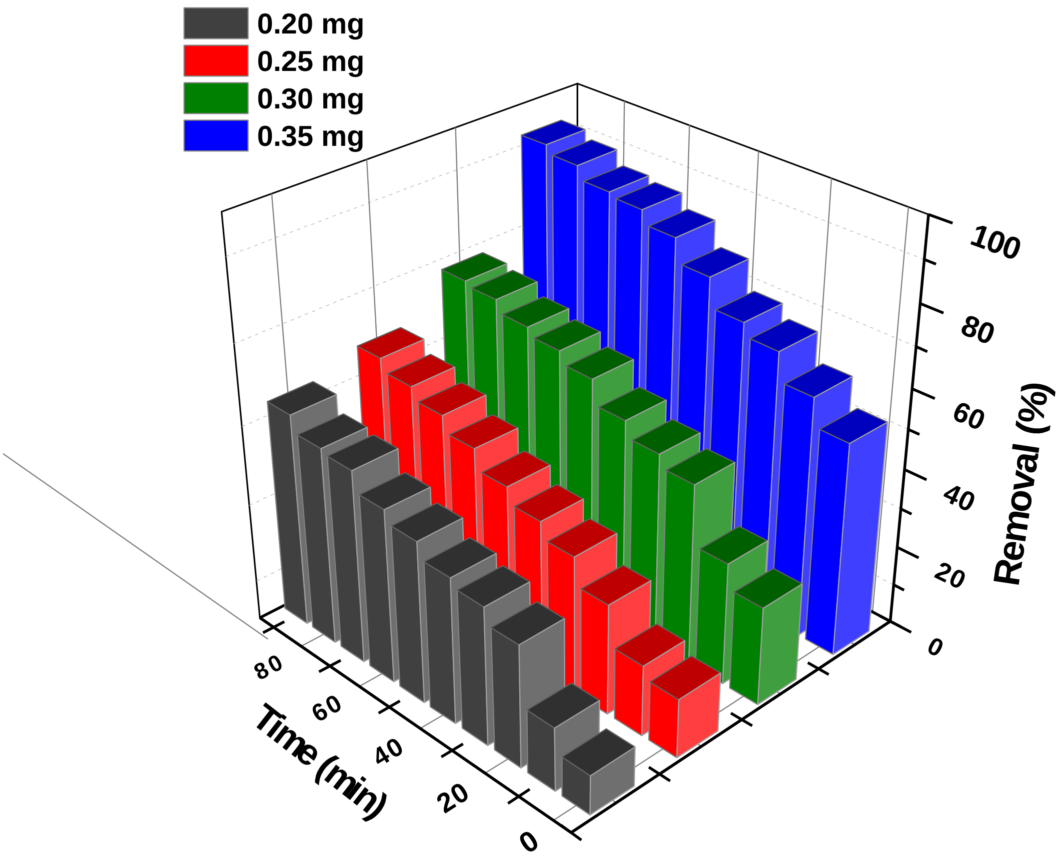

Fig. 9. Effect of photocatalyst concentrations on the percentage removal of MR dye with GO-CuO nanocomposites.

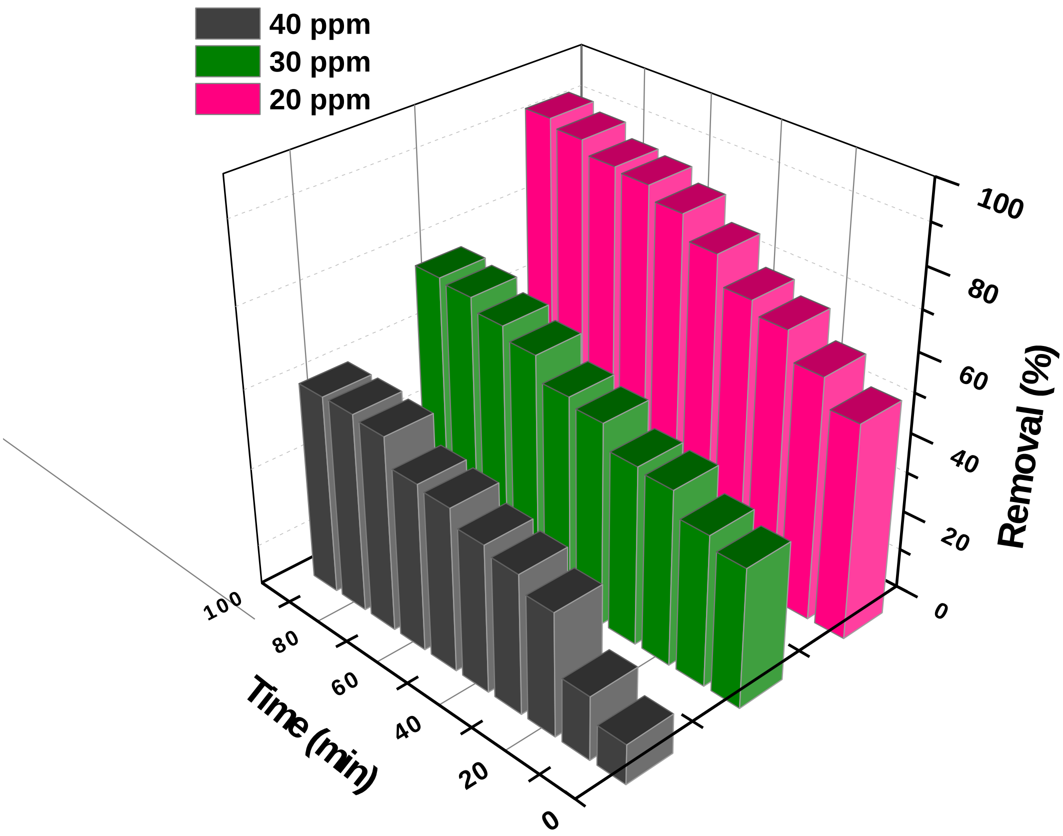

Fig.10. Effect of initial dye concentrations on the percentage removal of MR dye with GO-CuO nanocomposites**.**

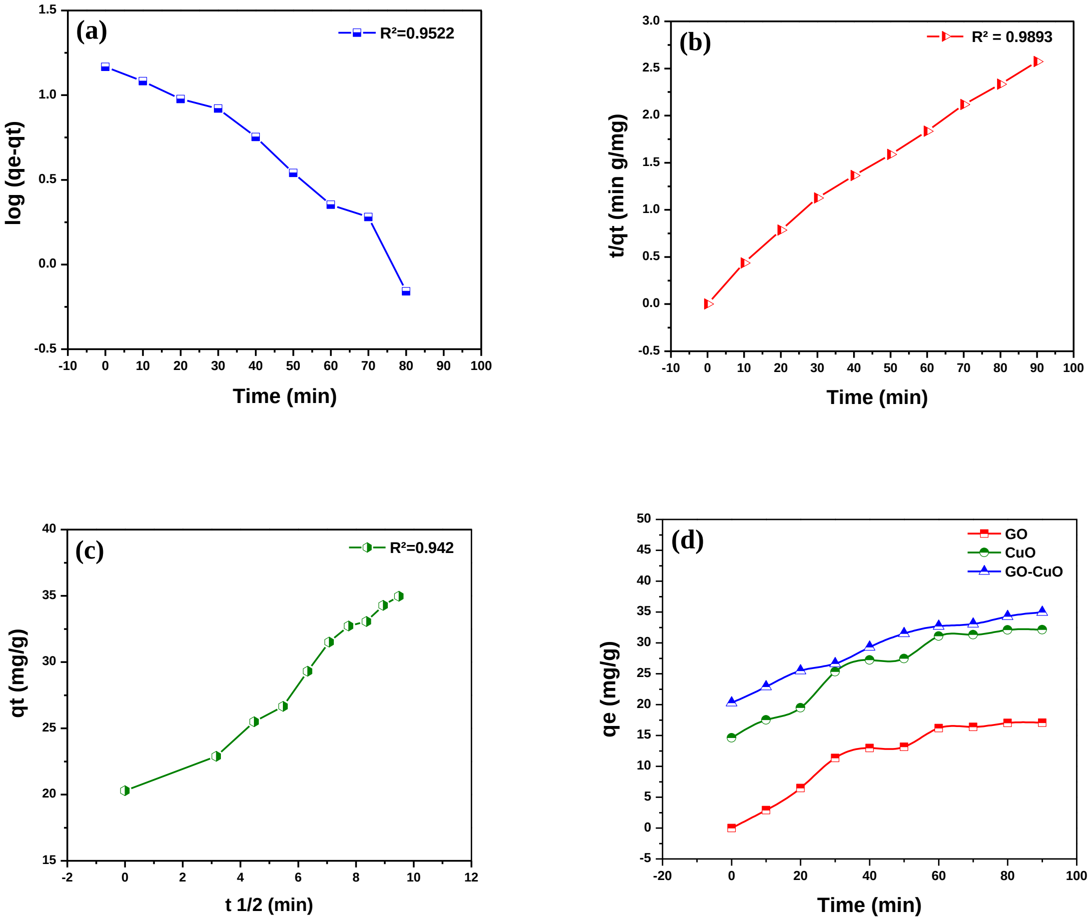

Fig. 11. Kinetic models of adsorption under optimized conditions (pH=8.0, [MR]=20 ppm, Catalyst=0.35 mg, agitation time 0–90 min and temperature = 35 °C) for; (a) pseudo-first-order model (b) pseudo-second-order (c) intraparticle diffusion model onto GO-CuO and (d) sorption capacities of GO, CuO and GO-CuO.

668

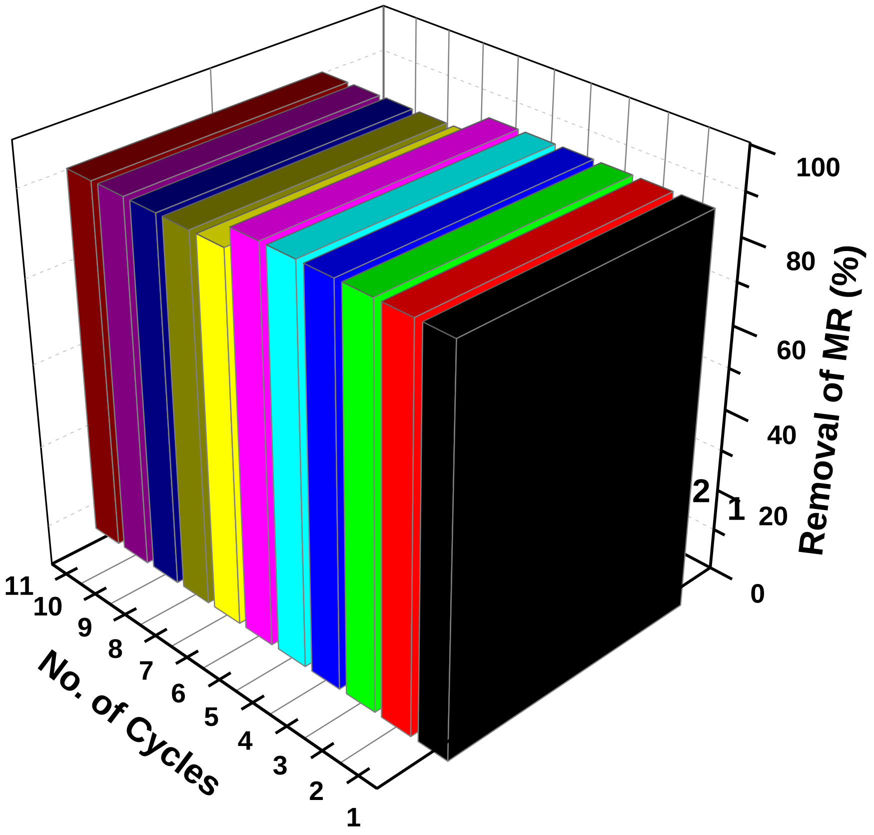

669
670 **Fig. 12.** Reusability of GO-CuO nanocomposite.
671

Graphical Abstract